

Impact of the activation rate of the hyperpolarization-activated current I_h on the neuronal membrane time constant and synaptic potential duration

Cesar C. Ceballos^{1,2}, Rodrigo F.O. Pena^{1,3}, and Antonio C. Roque^{1*}

¹Department of Physics, School of Philosophy, Sciences and Letters of Ribeirão Preto, University of São Paulo, Ribeirão Preto, SP, Brazil. ²Current address: Vollum Institute, Oregon Health & Science University, Portland, OR, USA. ³Current address: Federated Department of Biological Sciences, New Jersey Institute of Technology and Rutgers University, Newark, New Jersey, NJ, USA.

Abstract

The temporal dynamics of membrane voltage changes in neurons is controlled by ionic currents. These currents are characterized by two main properties: conductance and kinetics. The hyperpolarization-activated current (I_h) strongly modulates subthreshold potential changes by shortening the excitatory postsynaptic potentials and decreasing their temporal summation. Whereas the shortening of the synaptic potentials caused by the I_h conductance is well understood, the role of the I_h kinetics remains unclear. Here, we use a model of the I_h current model with either fast or slow kinetics to determine its influence on the membrane time constant (τ_m) of a CA1 pyramidal cell model. Our simulation results show that the I_h with fast kinetics decreases τ_m and attenuates and shortens the excitatory postsynaptic potentials more than the slow I_h . We conclude that the I_h activation kinetics is able to modulate τ_m and the temporal properties of excitatory postsynaptic potentials (EPSPs) in CA1 pyramidal cells. In order to elucidate the mechanisms by which I_h kinetics controls τ_m , we propose a new concept called “time scaling factor”. Our main finding is that the I_h kinetics influences τ_m by modulating the contribution of the I_h derivative conductance to τ_m .

1. INTRODUCTION

Hyperpolarization-activated cyclic nucleotide-gated (HCN) channels are non-selective cationic channels that underlie the hyperpolarization-activated cation current (I_h). These channels are the main controllers of synaptic integration at the distal dendrites in cortical and hippocampal neurons, where they are mostly expressed [1-3]. Similarly to K^+ channels, the HCN channel is a tetramer, made of the different combinations of subunits 1-4 [4,5], which leads to a diverse set of kinetics [4,6,7]. The subunit HCN1 presents the fastest kinetics of all four [4,6,7,8], and down regulation of HCN1 channels results in an increase in postsynaptic excitability [5,9,10,11,12,13,14,15].

The HCN1 and HCN2 isoforms are predominantly expressed in the dendrites of cortical and hippocampal pyramidal neurons. They are particularly suited to attenuate and shorten the excitatory postsynaptic potentials (EPSPs) of those cells [2]. Accordingly, pharmacological inhibition of I_h was found to increase summation of EPSPs [9,16,17] and genetic HCN1 deletion has been shown to be associated to lengthening of EPSPs in cortical and hippocampal pyramidal neurons [18,19]. Specific loss of the fast HCN1 subunit reduces I_h and slows down the activation/deactivation kinetics of I_h , prolonging the EPSP decay and increasing their temporal summation window [2,14,15,20,21].

The membrane time constant (τ_m) reflects the charging of the membrane capacitor and is traditionally thought to be determined only by the conductance of the subthreshold currents (linear and voltage dependent). In a purely passive membrane, the leak conductance determines τ_m in a manner such as the bigger the leak conductance the smaller τ_m . However, neurons also express voltage dependent currents with specific activation/deactivation kinetics providing them with a variety of dynamical temporal adjustments [4,22,23]. Surprisingly, the effect of the current kinetics has been long neglected and thought not connected to τ_m . Although Koch et al. [23] proposed that voltage-dependent currents would be able to modulate τ_m in a more complex manner than classical passive currents, there were no recent significant advances in the understanding of how I_h kinetics affects τ_m .

The activation time constant of I_h (τ_h) lies in a range from tens of milliseconds to several seconds and is well fitted by the sum of two exponentials with fast and slow time constants [4]. This might be related to the expression of at least two different subunits of HCN channels such as HCN1 and HCN2 in cortical neurons [4,24,25,26]. Here we ask whether and how the fast and slow kinetics of I_h contributes to τ_m as well as how these contributions would differ. In the positive case, we hypothesize that the faster activation would

* antonior@usp.br

decrease τ_m more strongly than the slow activation. For this, we use an I_h current model with either fast or slow τ_h embedded in a single compartment CA1 pyramidal neuron model. The model is composed of a leak current and the I_h current. Our results show that I_h with fast τ_h decreases τ_m and shortens artificial EPSPs in a stronger manner than I_h with slow τ_h . Furthermore, we also elucidate the mechanisms by which I_h with fast kinetics decreases more τ_m than the slow I_h . In order to elucidate the biophysical mechanisms underlying the influence of τ_h on τ_m , we propose a new analytical solution of the τ_m as an extension of the definition of τ_m from the classical passive cable theory.

2. METHODS

2.1. Neuron model

In our model, we consider a single compartment neuron model where the membrane voltage is described by the equation

$$C \frac{dV}{dt} = -I_h - I_L + I(t), \quad (1)$$

where C is the membrane capacitance, I_h is the hyperpolarization-activated current, I_L is the leak current, and $I(t)$ is an external current. The I_h current is modeled using the Hodgkin-Huxley formalism as:

$$I_h = \bar{g}_h A_h(V, t)(V - E_h), \quad (2)$$

where the maximum conductance \bar{g}_h is in nS and the reversal potential E_h is in mV.

The activation variable A_h is represented by the Boltzmann term [27]:

$$\frac{dA_h(V, t)}{dt} = \frac{A_h^\infty - A_h(V, t)}{\tau_h}, \quad (3)$$

where τ_h is the activation time constant in ms and A_h^∞ is the steady state activation variable described by

$$A_h^\infty = \frac{1}{1 + e^{(V - V_{1/2})/k}}. \quad (4)$$

In Eq. 4 we used $V_{1/2} = -82$ mV and $k = 9$ mV [2]. The leak conductance is modeled by the equation $I_L = \bar{g}_L(V - E_L)$ where \bar{g}_L is the maximum conductance in nS and E_L is the reversal potential in mV.

The input conductance G_m , or *slope* conductance (since it corresponds to the slope of the steady-state I - V relation) of the model is obtained by differentiating the total current in Eq. 1 with respect to V in the steady state, i.e., when $dV/dt = 0$. Since the total current in this case is $I = I_h + I_L$, we have

$$G_{in} = \frac{dI}{dV} = G_h + g_L, \quad (5)$$

where G_h is the slope conductance of the I_h current and g_L is the leak conductance.

The I_h slope conductance is obtained differentiating the current in Eq. 2

$$G_h = \frac{dI_h}{dV_{ss}} = \bar{g}_h A_h^\infty + \bar{g}_h (V - E_h) \frac{d(A_h^\infty)}{dV_{ss}}, \quad (6)$$

where the first term is the chord conductance (g_h) and the second term is the derivative conductance (G_h^{Der}) [28,29,30]. The derivative of $A_h^\infty(V)$ in Eq. 6 can be obtained differentiating Eq. 4: $\frac{dA_h^\infty}{dV} = \frac{(A_h^\infty - 1)A_h^\infty}{k}$, which implies that the derivative conductance is:

$$G_h^{Der} = \bar{g}_h A_h^\infty \frac{(A_h^\infty - 1)}{k} (V - E_h). \quad (7)$$

Notice that the chord conductance ($g_h = I_h/(V - E_h)$) is always positive, whereas G_h^{Der} can be positive or negative.

The single compartment is a cylinder with length and basis diameter 70 μm . The maximum conductance and reversal potential of the I_h and I_L are, respectively $\bar{g}_h = 10$ nS and $E_h = -30$ mV; and $\bar{g}_L = 10$ nS and $E_L = -90$ mV. In our simulations of the model, the initial membrane potential was -90 mV and the time step was 0.1 ms. Simulations were run in the NEURON simulator [31] and the results were analyzed in MATLAB (THE MATHWORKS, Natick, MA). Table 1 summarizes the nomenclature used to represent the conductances and Fig 1A shows their numerical properties. Also Fig 1B and Fig 1C shows the numerical properties of the steady state activation variable A_h^∞ .

Symbol	Definition
\bar{g}_L	Leak maximum conductance
\bar{g}_h	I_h maximum conductance
g_h	I_h chord conductance
G_h^{Der}	I_h derivative conductance
G_h	I_h slope conductance

Table 1. Conductances appearing in the model.

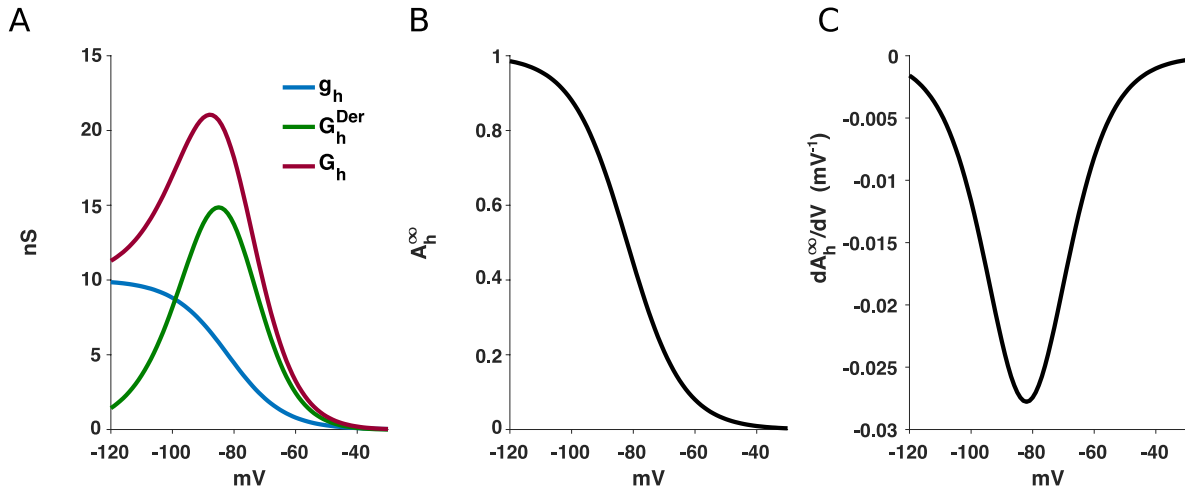


Fig 1. Voltage-dependent properties of the I_h . A. Slope conductance (G_h), chord conductance (g_h), and derivative conductance (G_h^{Der}). B. Steady state activation variable (A_h^∞). C. Voltage derivative of the steady state activation variable ($\frac{dA_h^\infty}{dV}$).

2.2. Simulation data analysis

The membrane time constant (τ_m) was determined from computational simulations analyzing voltage-current (V-I) relationships. V-I curves in current-clamp were obtained by injecting 4 s current pulses with +10 pA steps from -100 pA to 300 pA. Membrane time constant was measured by first applying 4 s long current to achieve the desired test potential and then injecting an additional small current step (+20 pA, 4 s) and fitting a single exponential to the initial rise of the voltage. Since simulations with I_h include sag, we fitted only from the initial rise voltage until the moment the maximum value was reached. Moreover, the effect of I_h on the amplitude and duration of EPSPs was determined by injecting a depolarizing EPSC at the end of the trace.

We also inject sinusoidal currents with linearly increasing frequencies (ZAP protocol) as in [29]. For that, the current $I = A \sin[\pi(f(t) - F_{start})(t - t_{start})]$ has its frequency described by $f(t) = F_{start} + \frac{(F_{stop} - F_{start})(t - t_{start})}{t_{stop} - t_{start}}$ where F_{start} (F_{stop}) is the initial (final) input frequency and t_{start} (t_{stop}) marks the initial (final) moment of current injection. Below we convert frequencies to ω , where $\omega = 2\pi f$. Standard values are $A = 10$ pA, $F_{start} = 0.001$ Hz and $F_{stop} = 40$ Hz, $t_{start} = 1$ s and $t_{stop} = 10$ s.

Data were analyzed using routines written in Matlab (THE MATHWORKS, Natick, MA) and figures were generated in GraphPad Prism (GRAPHPAD SOFTWARE, La Jolla, CA).

3. RESULTS

3.1. I_h kinetics affects EPSP attenuation

The main goal of this work was to determine the effect of the activation kinetics on the EPSP shape. It is well known that I_h attenuates and shortens EPSPs [2], however it still remains unknown how the I_h kinetics influences this attenuation. In order to test the effect of the I_h activation kinetics on the EPSP shape, we ran simulations where a fixed EPSC was applied in different membrane potentials. We ran simulations in a neuron with a single compartment with a leak current and I_h using two τ_h values: a fast one of 10 ms and a slow one of 500 ms. As expected, simulated EPSPs amplitude and area are decreased with hyperpolarized membrane potentials. This is caused by the increased g_h and G_h^{Der} due to hyperpolarization as it has been discussed elsewhere [29]. Interestingly, all the EPSP parameters were smaller when τ_h was faster (Fig 2B, 2C and 2D). These results suggest that the kinetics of I_h has a strong impact on the EPSP shape, with the I_h with fast activation kinetics being more efficient in attenuating the EPSPs than the I_h with slower kinetics.

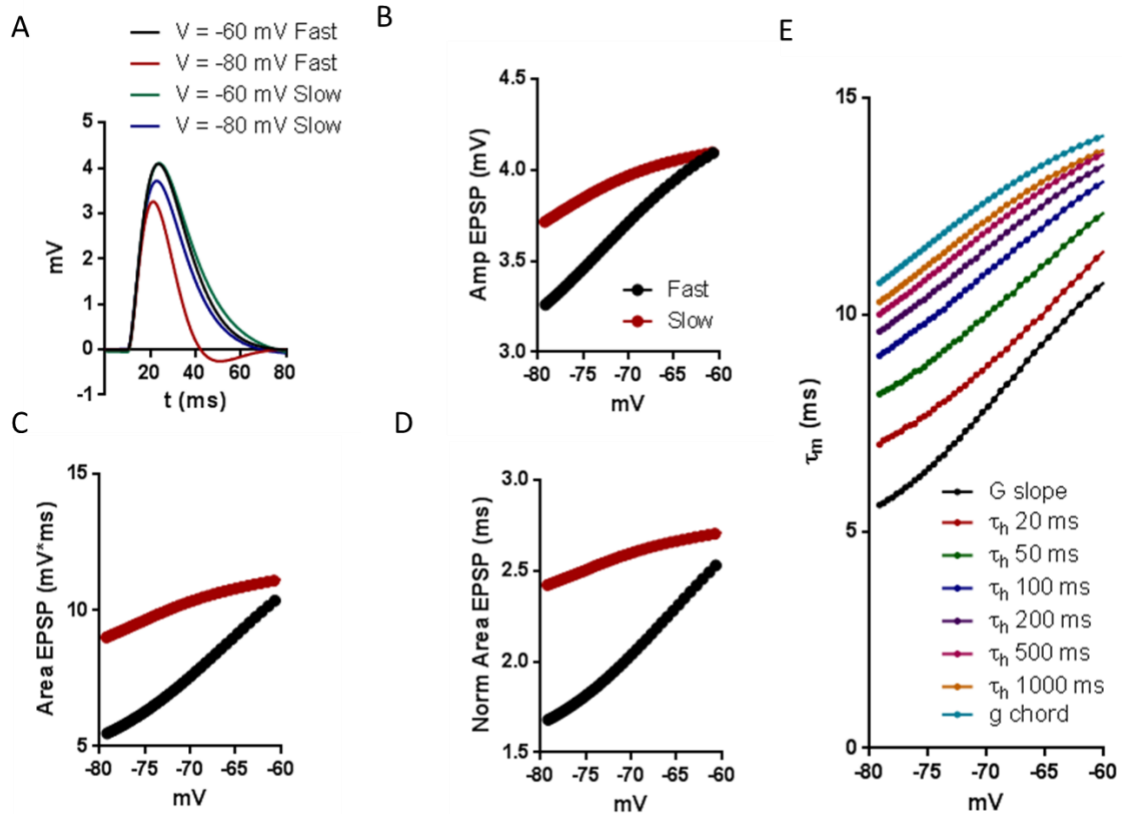


Fig 2. A. simulated EPSP representatives for membrane potentials -60 and -80 mV and for fast and slow τ_h . B. simulated EPSP amplitude obtained with I_h with fast activation ($\tau_h = 10$ ms) and slow activation ($\tau_h = 500$ ms) for different membrane potentials. C. EPSP area D. EPSP area normalized by the amplitude. E. Computational simulations for a single compartment with a leak current and I_h . Voltage dependent effect on

τ_m of τ_h with activation kinetics of 20, 50, 100, 200, 500 and 1000 ms. We also calculated $\tau_m = CR_{in}$ (G slope) and $\tau_m = C/(\bar{g}_L + g_h)$ (g chord).

The EPSP decay is mainly determined by τ_m [28]. In Fig 2A-D, we observe that I_h with fast kinetics shortens the EPSP decay more than I_h with slower kinetics. Based on these results, we hypothesize that I_h activation kinetics (τ_h) might influence the EPSP decay by influencing τ_m . In order to study the effect of τ_h on τ_m , we ran simulations of a single compartment neuron with a leak current and I_h , and then varied τ_h from 20 ms to 1000 ms. Fig 2E shows the voltage dependence of τ_m for different values of τ_h . As expected, τ_m decreases with hyperpolarization, i.e., τ_m decreases in the same direction of I_h activation. Furthermore, for a given membrane potential, τ_m decreases when τ_h decreases, suggesting that increasing the activation rate of I_h will consequently increase the rate of change of membrane potential. We can then conclude that I_h kinetics shortens the EPSPs by decreasing τ_m . In addition, notice that for any value of τ_h , τ_m is restricted to some limits, i.e. for $\tau_h \rightarrow 0$ we have $\tau_m = CR_{in}$ and for $\tau_h \rightarrow \infty$ we have $\tau_m = C/(g_L + g_h)$, where R_{in} is the steady state input resistance. Thus, we conclude that maximum EPSP attenuation is reached when $\tau_h = 0$ and the minimum when $\tau_h \rightarrow \infty$.

I_h modulation of the neuron temporal dynamics strongly depends on the voltage change speed [29]. As an example, note that EPSP amplitude and area curves (Figs. 2B-D) get closer for depolarized voltages than τ_m curves (Fig 2E). This is owing to the fact that I_h behaves as a high-pass filter causing a much stronger effect in voltage changes that evolve slowly (as the voltage changes used to measure τ_m) compared to faster events as EPSPs. Also, this effect is stronger when I_h is more activated (see Fig 1B).

Moreover, similar normalized areas of EPSPs were obtained under similar τ_m values (e.g. ~ 2.4 for normalized area of EPSPs at -80 mV for slow and at -63 mV for fast τ_h (Fig 2D) and their corresponding τ_h values ($\tau_m \approx 10$ ms, see Fig 1E)). This suggests that the observed changes in EPSPs temporal properties are likely caused by changes in τ_m . To confirm this, we ran simulations by changing g_L , g_h and the capacitance while computing τ_m and the normalized EPSP area.. Fig 3 shows good linear fits between τ_m and the normalized EPSP area, suggesting that changes in τ_m will lead to changes in EPSP temporal properties, regardless of the source of this variation (i.e., changes in conductance or capacitance).

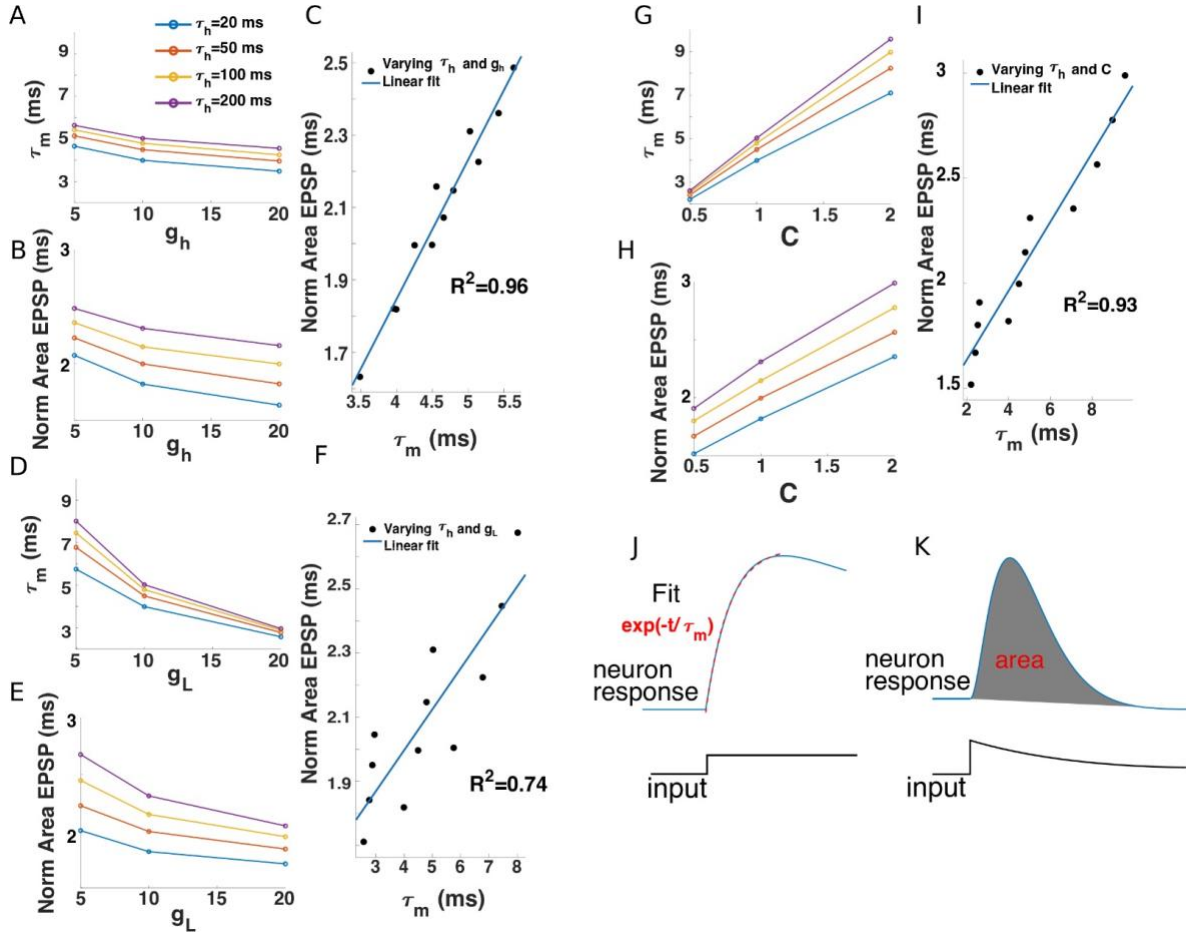


Fig 3. EPSP shortening is mediated by τ_m . (A,D,G) τ_m as function of g_h (in A), g_L (in E), C (in G), and τ_h (in all). (B,E,H) EPSP area normalized by the amplitude as function of g_h (in B), g_L (in E), C (in H), and τ_h (in all). (C,F,I) Linear fit of normalized area plotted against τ_m for each of the cases where g_h , g_L , and C are respectively varied with τ_h . Values of R^2 can be found in the plots. (J) τ_m was obtained by fitting the voltage change driven by square input current as a single exponential function. (K) EPSP area was calculated as the area under the trace.

3.2. Time scaling factor mediates modulation of the membrane time constant by rate of activation of I_h

In the previous section, by using computer simulations we established that I_h with fast kinetics shortens the EPSP decay more efficiently than I_h with slower kinetics, and that this is caused by an effect on τ_m . However, the biophysical mechanism underlying this influence of τ_h on τ_m remains unclear. To shed some light on this mechanism, we introduce a new concept, which we will call “time scaling factor”, or simply α factor.

The concepts of chord conductance and slope conductance are fundamental to explain the effect of I_h with infinitely slow or instantaneous activation, i.e., when $\tau_h \rightarrow \infty$ or $\tau_h \rightarrow 0$, on τ_m . For instance, in a single compartment neuron with a leak current (I_L) and I_h current, when $\tau_m(\tau_h \rightarrow \infty) = \frac{C}{\bar{g}_L + g_h}$, on the other hand, when $\tau_h = 0$, $\tau_m = \frac{C}{\bar{g}_L + G_h}$, where g_h is the I_h chord conductance and G_h is the I_h slope conductance (see Appendix A, Eq. A9 and A10, also see [22]). In summary, τ_m is determined by the steady state slope conductance of the instantaneous current and chord conductance of the infinitely slow current.

In a more general manner, τ_m can be expressed as $\tau_m = \frac{C}{\bar{g}_L + \bar{g}_h A_h^\infty + \bar{g}_h (V - E_h) \frac{\partial A_h}{\partial V}}$ (see Appendix A, Eq A8).

To gain a deeper insight, we made a simple characterization of $\frac{\partial A_h}{\partial V}$ and its dependency with τ_h . For this, we

ran simulations in which we injected a ZAP stimulus (see Methods), and we measured simultaneously ΔA_h and ΔV from the $A_h - V$ trajectories selected at specific slow ($\omega \approx 5$ Hz) and fast frequencies ($\omega \approx 200$ Hz) (Fig 4). The membrane potential was fixed with an external constant current so that the steady voltage is at $V = -80$ mV and we changed the value of $\tau_h = 100, 200, 500$ and 1000 ms. Our results showed almost vertical trajectories at low frequencies (Fig 4A), but evolving into horizontal and less round at higher frequencies (as in Fig 4 B) (we refer the reader to [29] for a thorough discussion of this phenomenon with this very same model and its implication in subthreshold resonance). This can be interpreted as large ΔA_h and ΔV at low frequencies that evolve into smaller ΔA_h and ΔV (Fig 4C and 4D). As expected, resonant behavior can be observed in Fig 4C, where for a particular frequency there is an amplification of the voltage response. Finally, Fig. 4E shows the behavior of $\frac{\Delta A_h}{\Delta V}$, increasing when τ_h decreases by the combined effect of larger ΔA_h and smaller ΔV for shorter τ_h .

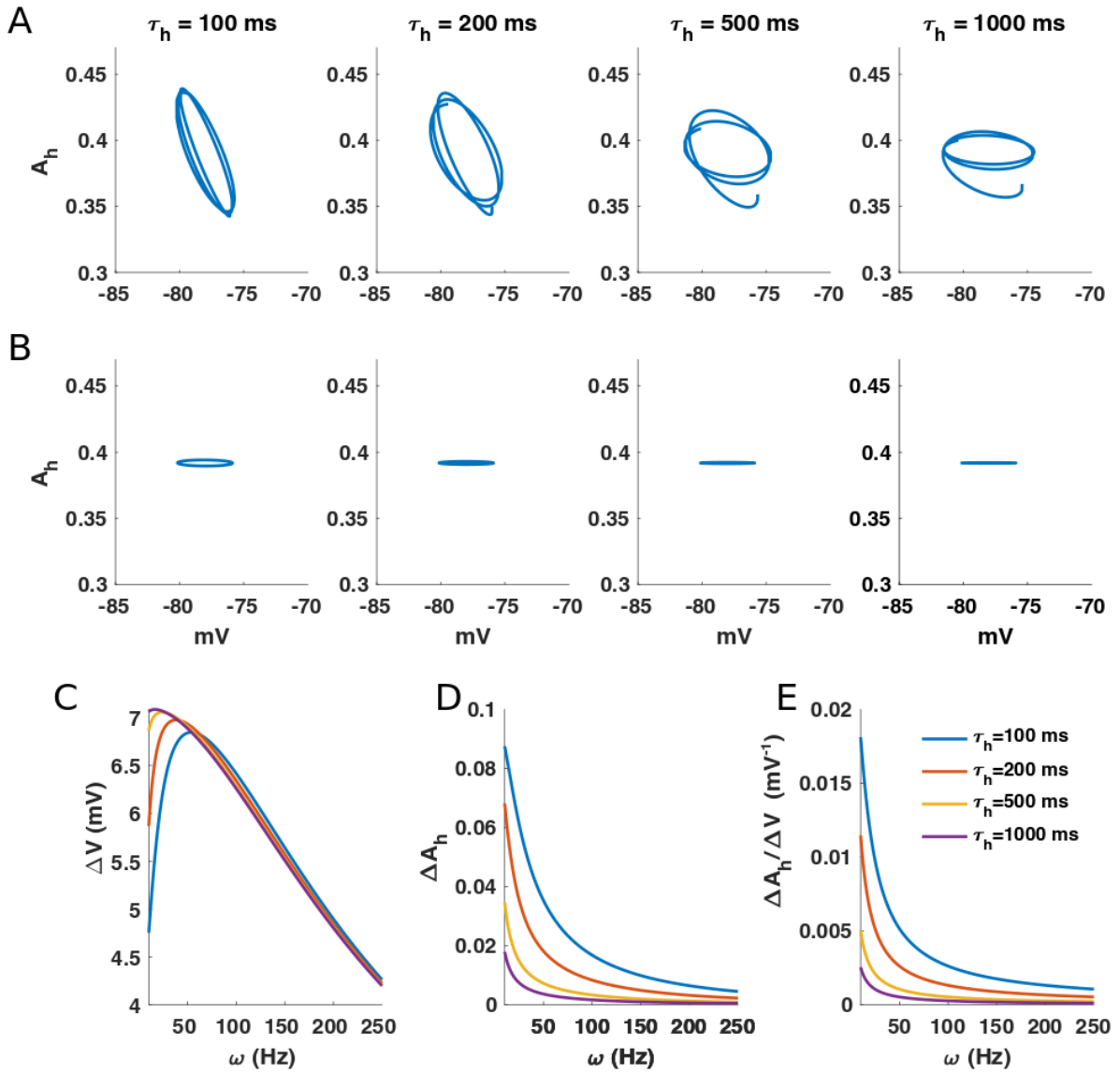


Fig 4. Evolution of trajectories for different τ_h . The plots contain activation variable (A_h) versus membrane potential of the neuron while being driven by ZAP stimulus for different activation time constants: $\tau_h = 100, 200, 500$ and 1000 ms. There are different stimulation frequencies (ω): (A) low frequency ($\omega \approx 5$ Hz) and (B)

high frequency ($\omega \approx 200$ Hz). (C) Variation of V (ΔV), (D) variation of A_h (ΔA_h), and (E) $\Delta A_h/\Delta V$ for different values of τ_h .

The partial derivative ($\frac{\partial A_h}{\partial V}$) in the third term of the denominator has well known analytical solution only for the extreme cases when $\tau_h \rightarrow \infty$ (infinitely slow kinetics) and $\tau_h = 0$ (instantaneous kinetics), as shown above. In order to obtain an analytical approximation of τ_m for any τ_h , that fits the behavior observed in Fig 4E, we propose an approximation of $\frac{\partial A_h}{\partial V}$. For this, we assume that a change in the voltage produces a change in the activation variable A_h that evolves in time following an exponential function [32]; $\frac{\partial A_h}{\partial V} = (1 - e^{-\Delta t/\tau_h}) \frac{\partial A_h^\infty}{\partial V}$. See from Fig 5 that the change in I_h activation (∂A_h) is limited by the available time to evolve (represented by Δt). With enough time, ∂A_h can achieve ∂A_h^∞ , otherwise ∂A_h is just a portion of ∂A_h^∞ . In that sense, the main effect of the interplay between Δt and τ_h on A_h is to partially activate I_h (Fig 5).

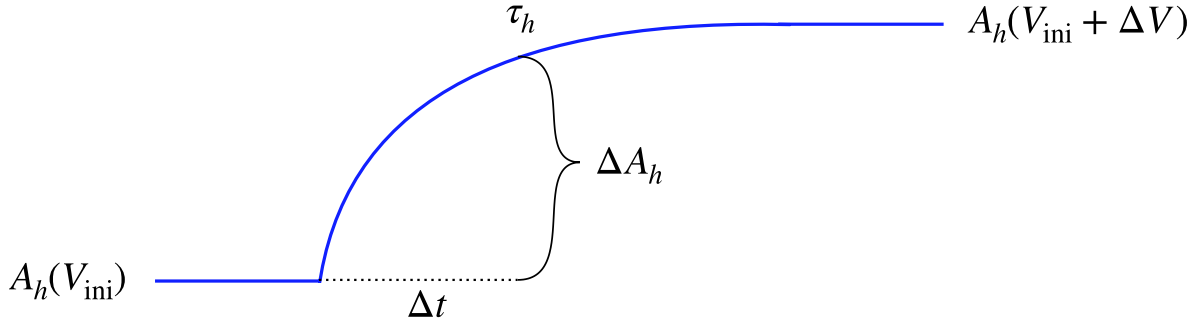


Fig 5. Schematic diagram of ΔA_h evolution over time. For the same Δt , ΔA_h is bigger for lower τ_h .

The time interval Δt in which changes in A_h have an influence on τ_m is also τ_m . In a single compartment with a leak current plus I_h , the longest τ_m corresponds to the case when all I_h contributions are neglected, i.e., when $\tau_m = \tau_L = C/\bar{g}_L$. Thus, we approximate the equation above to this case as follows: $\frac{\partial A_h}{\partial V} = (1 - e^{-\tau_L/\tau_h}) \frac{\partial A_h^\infty}{\partial V}$. The term

$$\alpha(\tau_L, \tau_h) = (1 - e^{-\tau_L/\tau_h}), \quad (8)$$

will be called “time scaling” (or α) factor.. Eq. 8 is extremely valuable since it provides a general understanding about the interaction of the temporal dynamics imposed by the passive current (τ_L) and the I_h kinetics (τ_h) currents as well as how this interaction determines the α factor. To verify its consistency, we check it using two scenarios. The first is when $\tau_h \rightarrow 0$, then $e^{-\tau_L/\tau_h} \rightarrow 0$, and $\alpha \rightarrow 1$. The second is when $\tau_h \rightarrow \infty$, then $e^{-\tau_L/\tau_h} \rightarrow 1$, and $\alpha \rightarrow 0$. Both results were expected, confirming the consistency of the α time scaling factor.

Thus, an approximate solution for τ_m can be expressed as: $\tau_m = \frac{C}{\bar{g}_L + \bar{g}_h A_h^\infty + \alpha \bar{g}_h (V - E_h) \frac{\partial A_h^\infty}{\partial V}}$, where the term

$\alpha \bar{g}_h (V - E_h) \frac{\partial A_h^\infty}{\partial V} = \alpha G_h^{Der}$. Writing the equation in a simpler manner:

$$\tau_m = \frac{C}{\bar{g}_L + \bar{g}_h + \alpha(\tau_h) G_h^{Der}}. \quad (9)$$

The α factor is dependent on τ_h in a way that when $\tau_h \rightarrow 0$ we have $\alpha \rightarrow 1$ and when $\tau_h \rightarrow \infty$ we have $\alpha \rightarrow 0$. However, the dependency of the α factor with τ_h , and whether this is the only factor determining it remains unknown. Therefore, in order to gain a deeper insight of the effect of τ_h on τ_m , we must first characterize the α factor.

This mathematical analysis allows us to conclude that the activation time constant (τ_h) is able to influence τ_m by modulating the contribution of the derivative conductance G_h^{Der} to the τ_m by changing the values of the α factor from 0 to 1 when τ_h changes from infinity to zero.

In the next sections we will use simulations in order to obtain an empirical form for the α factor. This new concept will be useful to reproduce quantitatively the effect of the I_h with different τ_h constants on τ_m .

3.3. The α factor is mostly affected by the leak membrane time constant

As discussed before, I_h has activation time constant values ranging from tens of milliseconds to several seconds. In this regard, I_h cannot be treated as an instantaneous or infinitely slow current. In order to study the effect of τ_h on τ_m , we must first characterize the α factor. To this end, in this section we will focus on the characterization of the α factor. Thus, we ran simulations of a single compartment with a leak current and I_h , and then we vary τ_h from 20 ms to 1000 ms as we did in Fig 2E.

In order to isolate the values of the α factor, we used the relationship $\tau_m = C/(\bar{g}_L + g_h + \alpha(\tau_h) G_h^{Der})$. The procedure adopted to obtain the values of α is the following: assuming the relationship $\tau_m = C/(\bar{g}_L + g_h + Y(V, \tau_h) G_h^{Der})$, we isolated $Y(V, \tau_h)$ and obtained its values using the values of τ_m measured from the simulations, the values of G_h^{Der} and g_h were obtained from Eqs. 6 and 7 and $\bar{g}_L = 10$ nS and $C = 154$ pF. Hence, $Y(V, \tau_h) = (C/\tau_m - \bar{g}_L - g_h)/G_h^{Der}$. Although $Y(V, \tau_h)$ clearly displays a voltage dependent relation (Fig 6A), for the sake of simplicity, we approximate the α factor as the averaged value of $Y(V)$, with which we can obtain a voltage independent expression for α (Fig 6B). In that way, the α factor is a nonlinear monotonic decreasing function of τ_h .

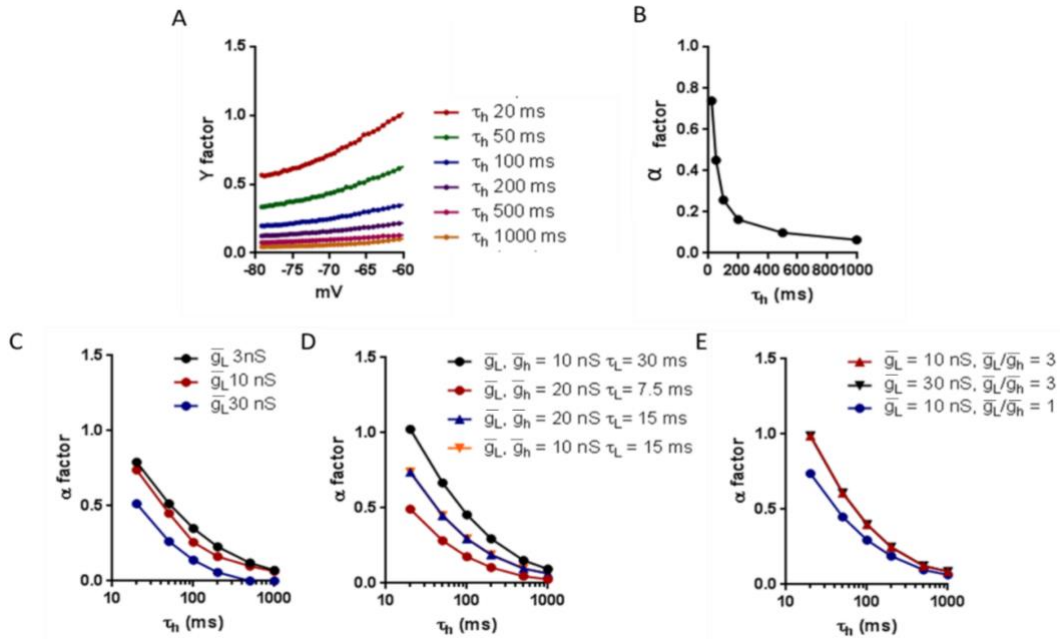


Fig 6. Computational simulations for a single compartment with a leak current and I_h with τ_h 20, 50, 100, 200, 500 and 1000 ms. A. We calculated the $Y(V)$ values using the relationship $Y(V) = (C/\tau_m - \bar{g}_L - g_h)/G_h^{Der}$. B. α factor values obtained from the relationship $\alpha = \text{mean}(Y(V))$. C. α factor obtained from simulations with $\bar{g}_h = 10$ nS and \bar{g}_L with values 3, 10 and 30 nS. D. α factor obtained from simulations with $\bar{g}_L = \bar{g}_h = 10$ or 20 nS and with τ_L values 30, 7.5 and 15 ms. E. α factor obtained from simulations with $\bar{g}_L = \bar{g}_h = 3, 10$ or 30 nS and with the ratio \bar{g}_L/\bar{g}_h values 1 and 3.

Intuitively, it is expected that the effects of τ_h on I_h activation might strongly depend on the temporal filtering imposed by the passive conductance. For instance, for a voltage change, if $\tau_h \gg \tau_m$, the I_h only changes partially but do not reach its steady state before the voltage steady state. In contrast, if $\tau_h \ll \tau_m$, then I_h fully changes, always reaching the steady state [29]. Thus, it seems reasonable to explore the dependency of the α factor with the passive properties. Then, once we isolate the α factor from simulations and characterize its dependency with τ_h , we will be able to further characterize the α factor in conditions when \bar{g}_L changes.

Therefore, we ran simulations of a single compartment with a leak current and I_h , with τ_h values from 20 to 1000 ms and with $\overline{g_L}$ values of 3, 10 and 30 nS.

In the previous section, we showed the analysis conducted in order to obtain the α factor with $\overline{g_L}$ and $\overline{g_h}$ values of 10 nS. Now, in order to determine if the α factor is affected by the value of the leak conductance $\overline{g_L}$, we ran two more simulations using $\overline{g_L} = 3$ and 30 nS. The curves of the α factor when $\overline{g_L} = 3$ nS and when $\overline{g_L} = 10$ nS are similar, but, when $\overline{g_L} = 30$ nS, the α factor reaches zero for smaller values of τ_h (Fig 6C). These results suggest that the α factor is a function of $\overline{g_L}$ in a manner that increasing $\overline{g_L}$ accelerates the decay of the α factor. Summarizing, our results suggest that increasing the leak conductance the α factor decreases consequently decreasing the impact of τ_h on τ_m .

The leak conductance ($\overline{g_L}$) can influence the α factor through different parameters: directly by the $\overline{g_L}$ value, indirectly through the ratio $\overline{g_L}/\overline{g_h}$, or by the membrane time constant of the leak conductance ($\tau_L = C/\overline{g_L}$). We established by which parameter the leak conductance influences the α factor through simulations in which we change $\overline{g_L}$, $\overline{g_h}$, C and τ_L . In these simulations, the values of $\overline{g_L}$ and $\overline{g_h}$ were the same in order to keep constant its ratio, i.e. $\overline{g_L}/\overline{g_h} = 1$. In total four combinations ($\overline{g_L}$, C, τ_L) were used: (10 nS, 300 pF, 30 ms), (20 nS, 150 pF, 7.5 ms), (20 nS, 300 pF, 15 ms), and (10 nS, 150 pF, 15 ms) (Fig 6D). The results show that whenever τ_L was fixed to a value (e.g. $\tau_L = 15$ ms) the α factor obtained was the same, independently of the values of $\overline{g_L}$ or $\overline{g_h}$, (Fig 6D). Moreover, when the $\overline{g_L}$ or $\overline{g_h}$ were fixed, the α factor was different whenever τ_L was different in a manner that the α factor was lower when τ_L was lower suggesting a correlation. Our observations suggest that the α factor is mostly dependent on τ_L , but not a function of $\overline{g_L}$ or $\overline{g_h}$.

Finally, we tested the effect of the ratio $\overline{g_L}/\overline{g_h}$ on the α factor. In this case, we simulated changes in the values of $\overline{g_L}$ and $\overline{g_h}$, keeping constant $\tau_L = 15$ ms (Fig 6E). Next, three combinations ($\overline{g_L}$, $\overline{g_L}/\overline{g_h}$) were used: (10 nS, 1), (10 nS, 3), and (30 nS, 3). The results showed that whenever the ratio $\overline{g_L}/\overline{g_h}$ was fixed (e.g. $\overline{g_L}/\overline{g_h} = 3$), the α factor obtained was the same, independently of the $\overline{g_L}$ or $\overline{g_h}$ values (Fig 6E). When $\overline{g_L}$ or the $\overline{g_h}$ value was fixed, the α factor was different when the ratio $\overline{g_L}/\overline{g_h}$ was different in a manner that the α factor was lower when the ratio $\overline{g_L}/\overline{g_h}$ was lower, also suggesting a correlation. Our observations suggest that the α factor is a function that depends on the ratio $\overline{g_L}/\overline{g_h}$.

As we have already mentioned, in Fig 6C when $\overline{g_L}$ value increases the α factor decreases. Interestingly, in Fig 6C, the values of $\overline{g_h}$ and C were kept constant, then when the $\overline{g_L}$ value was increased, simultaneously, the ratio $\overline{g_L}/\overline{g_h}$ also increased and τ_L decreased. However, our previous results (see above) showed that the α factor was lower when τ_L or the ratio $\overline{g_L}/\overline{g_h}$ was lower. This suggests that τ_L is a more influential parameter than the ratio $\overline{g_L}/\overline{g_h}$ in the determination of the α factor. Overall, the results in this section are important not only to understand the α factor dependencies but also to determine it from experimental setups.

3.4. Numerical predictions of τ_m using the α factor

In this section we validate our mathematical approximation by comparing it with simulations exploring the values of τ_h and τ_L . Figure 7 shows values of τ_m for different combinations of τ_h (20, 100 and 1000 ms) obtained from simulations and the τ_m values are predicted using Eqs. 8 and 9. For the combinations ($\overline{g_L}$, τ_L) we used: (3 nS, 45 ms), (10 nS, 15 ms) and (30 nS, 5 ms) (Fig 7A, 7B and 7C). Interestingly, the maximum difference of the τ_m between the simulated and the theoretical values were 3, 1.17, and 0.3 ms for $\tau_L = 45$, 15 and 5 ms, respectively, suggesting a good agreement between the approximation and the simulation. We conclude that approximating the α factor as an exponential function with the ratio τ_L/τ_h is sufficient to completely reproduce the quantitative tendencies of τ_m observed in the simulations.

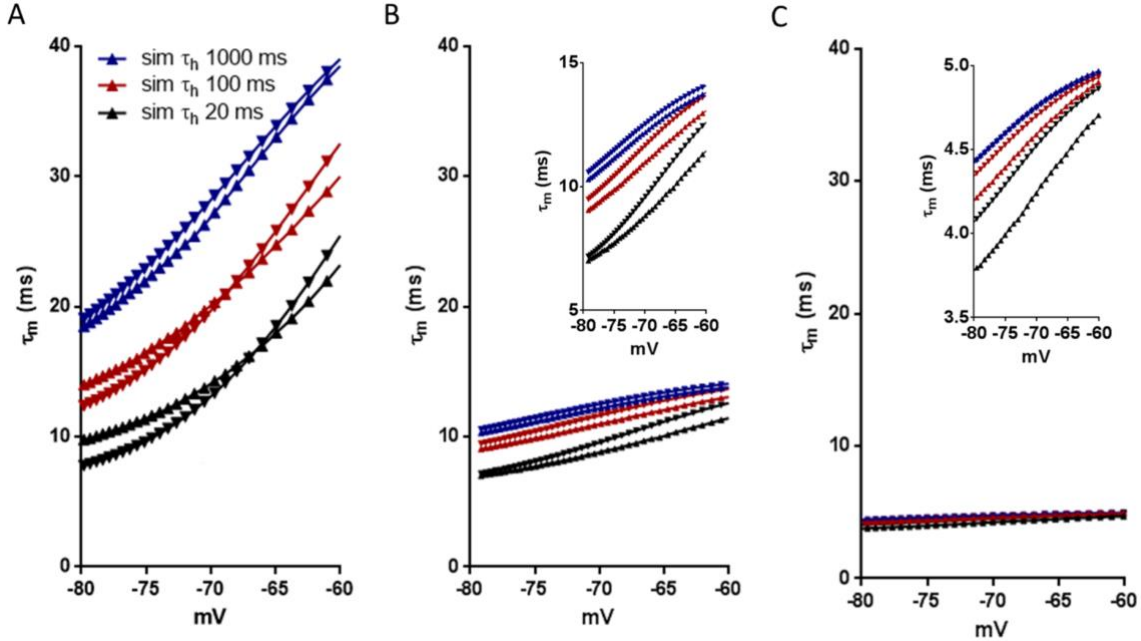


Fig 7. Computational simulations of a single compartment with a leak current and I_h with τ_h 20, 100 and 1000 ms. τ_m measured from the simulations are the triangle symbols. τ_m calculated by the relationship $\tau_m = C/(\bar{g}_L + g_h + \alpha(\tau_h) G_h^{Der})$ are the down triangle symbols, where the α factor was determined using $\alpha = 1 - \exp(-\tau_L/\tau_h)$. A. τ_m from simulations where $\tau_L = 45$ ms. B. The same as A but in this case $\tau_L = 15$ ms. C. The same as A but in this case $\tau_L = 5$ ms.

4. DISCUSSION

The aim of this work was to establish the role of hyperpolarization-activated current (I_h) kinetics on the membrane time constant (τ_m) of a neuron model, and on the shape of excitatory postsynaptic potentials (EPSPs) in this neuron. Our simulations showed that I_h with faster activation rates attenuates and shortens the EPSPs more efficiently than I_h with slower activation rates. Since one of the most important physiological effects of τ_m in neurons is the shape of the EPSPs, especially on its descending phase, we demonstrated that the influence of τ_h on τ_m is responsible for the influence of τ_h on the EPSP decay.

Accordingly, it has been demonstrated that an increase in conductance leads to a decrease in τ_m following a shortening of EPSPs which mostly affects its decay phase [33]. In addition, experimental and computational studies have shown that I_h mainly affects the decay phase of EPSPs rather than the rise phase [34, 35]). And it is well known that in simple point-neuron models, the EPSP decay phase is mostly determined by τ_m [36]. Moreover, we further confirmed that changes in τ_m are correlated with changes in EPSPs temporal properties, regardless of the source of these variations (e.g. changes in conductance, capacitance and I_h kinetics). Overall, we provide compelling evidence that I_h kinetics modulates the EPSP shape by its influence upon τ_m confirming a longstanding empirical observation.

It is well known that I_h can control membrane input resistance and the resting membrane potential (RMP) as well as the membrane time constant [37,38]. Our results suggest that I_h kinetics selectively modulates τ_m without affecting other neuronal properties such as the resting membrane potential and membrane input resistance, which are only determined by the I_h conductance. Thus, variations in the I_h activation/deactivation kinetics can selectively modulate the EPSPs shape and temporal properties of the neuron with undetected impact on other subthreshold properties (e.g. membrane input resistance or resting membrane potential).

In order to elucidate the biophysical mechanism underlying the influence of τ_h on τ_m , we proposed a new kinetics-dependent analytical solution of $\tau_m = C/(\bar{g}_L + g_h + \alpha(\tau_h) G_h^{Der})$, where the α factor is dependent on τ_h and τ_L . This last relationship establishes that the I_h derivative conductance G_h^{Der} contributes controlling the τ_m , although this control is limited by the α factor. In a previous work, Drion and colleagues studied the dynamical interplay among many different ionic currents in distinct timescales using the analysis of dynamic

input conductances [39]. The mathematical derivations in their work are conceptually similar to ours, mostly regarding the derivation of the α factor (called “voltage-dependent weighting factor” in [39]). Although we obtained a different mathematical expression, [39], the voltage-dependent weighting factor was defined as logarithmic distances among activation time constants whereas in ours we defined the α factor as an exponential function of the ratio τ_L/τ_h , we believe these definitions are mechanistically similar. Drion and colleagues used this approach to investigate the mechanisms of ion channel interplay in shaping suprathreshold activity (spikes), whereas we investigated the shaping of subthreshold activity (EPSPs and τ_m).

Importantly, we get a good agreement between the theoretical and simulated data using an approximation of the α factor that follows as an exponential function of the ratio τ_L/τ_h . The α factor is a nonlinear monotonic decreasing function of τ_h and an increasing function of τ_L . Then, decreasing τ_h increases the α factor values and consequently increases the impact of τ_h on τ_m . Moreover, increasing the leak conductance decreases τ_L which in turn decreases the α factor values and consequently decreases the impact of τ_h on τ_m .

Our theoretical predictions can be tested in real neurons using the dynamic clamp technique as being reported elsewhere [28,37]. For this, it is possible to study the effect of the I_h kinetics on neuron excitability injecting an artificial I_h in neurons using the Eq. 2, Eq. 3, and Eq. 4, and the values for maximum conductance \bar{g}_h , the reversal potential E_h and the activation time constant τ_h (fast and slow, respectively) which can be obtained from previous reports [37]. Furthermore, the α factor can be easily determined from voltage-clamp experiments by measuring the leak and I_h time constants (τ_L and τ_h).

Our results should also be valid and extended for multiple I_h currents. In fact, each current will have its own α factor determined from the set of τ_L and τ_h (see [40] for an example of experiments). Such an extension may give rise to new interpretations of how a neuron performs temporal integration of an input under the influence of multiple ionic current.

In conclusion, our results expand the membrane time constant definition from the classical passive cable equations and should be useful for further interpretations of processing employed by neurons when receiving synaptic inputs.

Acknowledgements

This article was produced as part of the IRTG 1740/TRP 2011/50151-0, funded by the DFG/FAPESP. It was also supported partially by the S. Paulo Research Foundation (FAPESP) Research, Innovation and Dissemination Center for Neuromathematics (CEPID NeuroMat, Grant No. 2013/07699-0). The authors also thank FAPESP support through Grants Nos. 2013/25667-8 (R.F.O.P.), 2015/50122-0 and 2018/20277 (A.C.R.). C.C.C. was supported by a CAPES PhD scholarship. A.C.R. thanks financial support from the National Council of Scientific and Technological Development (CNPq), Grant No. 306251/2014-0. This study was financed in part by the Coordenação de Aperfeiçoamento de Pessoal de Nível Superior-Brasil (CAPES) - Finance Code 001.

Author contribution statement

Author Contributions: C.C.C conceived the work, C.C.C. and R.F.O.P. run and analyze the simulations, C.C.C. and R.F.O.P and A.C.R. wrote the manuscript, A.C.R. supervised the research. All authors read and agreed to the published version of the manuscript.

REFERENCES

1. M. Maroso, G.G. Szabo, H.K. Kim, A. Alexander, A.D. Bui, S.H. Lee, B. Lutz, and I. Soltesz, *Neuron* **89**, (2016) 1059-1073.
2. J.C. Magee, *J. Neurosci.* **18**, (1998) 7613-7624.
3. C. Gasselín, Y. Inglebert, and D. Debanne, *J. Physiol.* **593**, (2015) 4855-4869.
4. K.A. Dougherty, D.A. Nicholson, L. Diaz, E.W. Buss, K.M. Neuman, D.M. Chetkovich, and D. Johnston, *J. Neurophysiol.* **109**, (2013) 1940-1953.
5. G.P. Brennan, T.Z. Baram, and N.P. Poolos, *Cold Spring Harb. Perspect. Med.* **6**, (2016) a022384.
6. T.M. Ishii, M. Takano, and H. Ohmori, *J. Physiol.* **537**, (2001) 93-100.
7. J. Stieber, A. Thomer, B. Much, A. Schneider, M. Biel, and F. Hofmann, *J. Biol. Chem.* **278**, (2003) 33672-33680.
8. O. Franz, B. Liss, A. Neu, J. Roeper, *Eur. J. Neurosci.* **12**, (2000) 2685–2693.

9. M.M. Shah, A.E. Anderson, V. Leung, X.D. Lin, D. Johnston, *Neuron* **44**, (2004) 495–508.
10. S. Jung, L.N. Warner, J. Pitsch, A.J. Becker, and N.P. Poolos, *J. Neurosci.* **31**, (2011) 14291-14295.
11. S. Jung, T.T. Jones, J.J. Lugo, A.H. Sheerin, J.W. Miller, R. D'Ambrosio, A.E. Anderson, N.P. Poolos, *J. Neurosci.* **27**, (2007) 13012–13021.
12. S. Jung, J.B. Bullis, I.H. Lau, T.D. Jones, L.N. Warner, N.P. Poolos, *J. Neurosci.* **30**, (2010) 6678–6688.
13. B. Marcelin, L. Chauviere, A. Becker, M. Migliore, M. Esclapez, C. Bernard, *Neurobiol. Dis.* **33**, (2009) 436–447.
14. U. Strauss, M.H. Kole, A.U. Bräuer, J. Pahnke, R. Bajorat, A. Rolfs, R. Nitsch, and R.A. Deisz, *Eur. J. Neurosci.* **19**, (2004) 3048-3058.
15. M.H. Kole, A.U., Bräuer, and G.J. Stuart, *J. Physiol.* **578**, (2007) 507-525.
16. T. Berger, M.E. Larkum, H.R. Luscher, *J. Neurophysiol.* **85**, (2001) 855–868.
17. N.P. Poolos, M. Migliore, D. Johnston, *Nat. Neurosci.* **5**, (2002) 767–774.
18. M.F. Nolan, G. Malleret, J.T. Dudman, D.L. Buhl, B. Santoro, E. Gibbs, S. Vronskaya, G. Buzsáki, S.A. Siegelbaum, E.R. Kandel, A. Morozov, *Cell* **119**, (2004) 719 –732.
19. D. Tsay, J.T. Dudman, S.A. Siegelbaum, *Neuron* **56**, (2007) 1076 –1089.
20. D.H. Brager and D. Johnston, *J. Neurosci.* **27**, (2007) 13926-13937.
21. K. Chen, I. Aradi, N. Thon, M. Eghbal-Ahmadi, T.Z. Baram, I. Soltesz, *Nat. Med.* **7**, (2001) 331–336.
22. M.W. Remme and J. Rinzal, *J. Comput. Neurosci* **31**, (2011) 13-30.
23. C. Koch, M. Rapp, and I. Segev, *Cereb. Cortex* **6**, (1996) 93-101.
24. R. Surges, T.M. Freiman, and T.J. Feuerstein, *Epilepsia* **44**, (2003): 150-156.
25. N.P. Poolos, J.B. Bullis, and M.K. Roth, *J. Neurosci.* **26**, (2006): 7995-8003.
26. I. van Welie, J.A. van Hooft, and J.W. Wytse, *P. Natl. Acad. Sci. USA* **101**, (2004): 5123-5128.
27. A.R. Willms, D.J. Baro, R.M. Harris-Warrick, and J. Guckenheimer, *J. Comput. Neurosci.* **6**, (1999) 145–168.
28. C.C. Ceballos, A.C. Roque, and R.M. Leão, *Biophys. J.* **113**, (2017) 2207-2217.
29. R.F.O. Pena, C.C. Ceballos, V. Lima, and A.C. Roque, *Phys. Rev. E* **97**, (2018) 042408.
30. C.C. Ceballos, R.F.O. Pena, A.C. Roque, R.M. Leão, *Channels* **12**, (2018) 81-88.
31. T. Carnevale and M. Hines, *The NEURON Book* (Cambridge University Press, Cambridge, UK, 2006).
32. T. Van Pottelbergh, G. Drion, R. Sepulchre, *Neural Comput.* **33**, (2021) 563-589.
33. A.I. Wlodarczyk, C. Xu, I. Song, M. Doronin, Y.W. Wu, M. Walker, and A. Semyanov, *Front. Neural Circuits* **7**, (2014) 205.
34. S. Liu and M. T Shipley, *J. Neurosci.* **28**, (2008) 10311-10322.
35. W.D. Anderson, E.J. Galván, J.C. Mauna, E. Thiels, G. Barrionuevo, *Pflugers Arch. - Eur. J. Physiol.* **462**, (2011) 895-912.
36. M.J. Richardson and G. Silberberg, *J. Neurophysiol.* **99**, (2008) 1020-1031.
37. C.C. Ceballos, S. Li, A.C. Roque, T. Tzounopoulos, and R.M. Leão, *Front. Cell. Neurosci.* **10**, (2016) 249.
38. J. Yamada-Hanff and B.P. Bean, *J. Neurophysiol.* **114**, (2015) 2376-2389.
39. G. Drion, A. Franci, J. Dethier, R. Sepulchre, *eNeuro* **2**, (2015) e0031-14.2015.
40. A.O.S. Cunha, C.C. Ceballos, J.L. de Deus, and R.M. Leão, *Eur. J. Neurosci.* **47**, (2018) 1401-1413.

Appendix A. Membrane time constant is modulated by rate of activation of I_h

A single compartment neuron with one leak current (I_L) and one I_h has the membrane equation:

$$C \frac{dV}{dt} = -I_L - I_h \quad (\text{A1})$$

And assuming that the voltage temporal evolution of the capacitor charging can be described by a single exponential function when a constant current step is injected [32]:

$$V(t) = B \left(1 - \exp\left(-\frac{t}{\tau_m}\right) \right) + V_0, \quad (\text{A2})$$

where B and V_0 are constants and τ_m is the membrane time constant. Then differentiating equation (A2) in time and multiplying by C :

$$C \frac{dV}{dt} = CB \left(\frac{e^{-\frac{t}{\tau_m}}}{\tau_m} \right) \quad (\text{A3})$$

Isolating the exponential term in Eq A2 we get that $e^{-\frac{t}{\tau_m}} = 1 - \frac{V(t)-V_0}{B}$, and substituting this in Eq (A3)

$$C \frac{dV}{dt} = CB \left(\frac{1 - \frac{V(t)-V_0}{B}}{\tau_m} \right) \quad (\text{A4})$$

Equating A4 and A1 and differentiating with respect to V :

$$\frac{C}{\tau_m} = \frac{\partial I_L}{\partial V} + \frac{\partial I_h}{\partial V} \quad (\text{A5})$$

Isolating τ_m :

$$\tau_m = \frac{C}{\frac{\partial I_L}{\partial V} + \frac{\partial I_h}{\partial V}} \quad (\text{A6})$$

Differentiating each current, we obtain:

$$\tau_m = \frac{C}{\bar{g}_L + \bar{g}_h A_h + \bar{g}_h (V - E_h) \frac{\partial A_h}{\partial V}} \quad (\text{A7})$$

For the sake of simplicity, we will only investigate the cases where ΔA_h is small due to small ΔV . Under this condition, $\bar{g}_h A_h \approx \bar{g}_h A_h^\infty$, where this term corresponds to the I_h chord conductance (g_h). Replacing in the equation:

$$\tau_m = \frac{C}{\bar{g}_L + \bar{g}_h A_h^\infty + \bar{g}_h (V - E_h) \frac{\partial A_h}{\partial V}} \quad (\text{A8})$$

The partial derivative $\left(\frac{\partial A_h}{\partial V}\right)$ in the third term of the denominator has well known analytical solution only for the extreme cases when $\tau_h \rightarrow \infty$ (infinitely slow kinetics) and $\tau_h = 0$ (instantaneous kinetics). When $\tau_h \rightarrow \infty$, A_h does not change with V , then $A_h = A_h^\infty(V_0)$ and $\frac{\partial A_h}{\partial V} = 0$, then:

$$\tau_m(\tau_h \rightarrow \infty) = \frac{C}{\bar{g}_L + \bar{g}_h A_h^\infty} = \frac{C}{\bar{g}_L + g_h} \quad (\text{A9})$$

On the other hand, when $\tau_h = 0$, $\frac{\partial A_h}{\partial V} = \frac{\partial A_h^\infty}{\partial V}$, then:

$$\tau_m = \frac{c}{\bar{g}_L + \bar{g}_h A_h^\infty + \bar{g}_h (V - E_h) \frac{\partial A_h^\infty}{\partial V}} = \frac{c}{\bar{g}_L + G_h} \quad (\text{A10})$$

Where G_h is the slope conductance (G_h). Concluding, we can state that τ_m is determined by the steady state slope conductance of the instantaneous current and chord conductance of the infinitely slow current.